Prediction of High-Pressure Adsorption Equilibrium of Supercritical Gases Using Density Functional Theory

Thanh X. Nguyen, Suresh K. Bhatia,* and David Nicholson

Division of Chemical Engineering, The University of Queensland, Brisbane, Queensland 4072, Australia

Received October 5, 2004. In Final Form: January 16, 2005

In this paper, we present the results of the prediction of the high-pressure adsorption equilibrium of supercritical gases (Ar, N_2, CH_4, and CO_2) on various activated carbons (BPL, PCB, and Norit R1 extra) at various temperatures using a density-functional-theory-based finite wall thickness (FWT) model. Pore size distribution results of the carbons are taken from our recent previous work,[1,2] using this approach for characterization. To validate the model, isotherms calculated from the density functional theory (DFT) approach are comprehensively verified against those determined by grand canonical Monte Carlo (GCMC) simulation, before the theoretical adsorption isotherms of these investigated carbons calculated by the model are compared with the experimental adsorption measurements of the carbons. We illustrate the accuracy and consistency of the FWT model for the prediction of adsorption isotherms of the all investigated gases. The pore network connectivity problem occurring in the examined carbons is also discussed, and on the basis of the success of the predictions assuming a similar pore size distribution for accessible and inaccessible regions, it is suggested that this is largely related to the disordered nature of the carbon.

1. Introduction

High-pressure adsorption of supercritical gases in porous carbons is involved in numerous industrial applications related to gas separation and gas storage. A good understanding of this subject is also crucial to several more recent applications such as coal bed methane recovery and carbon dioxide sequestration for greenhouse gas mitigation. Successful prediction of the high-pressure adsorption of supercritical gases having different molecular sizes and shapes is also important for unambiguous understanding of the carbon internal structure as well as of the physical behavior of confined fluids in the presence of the adsorption force field of the carbon. Such prediction is possible based on structural characteristics probed using low-temperature adsorption,[1,2] but little effort in this direction has been made.

In recent years, significant progress in molecular theories such as nonlocal density functional theory (NLDFT)[3−6] and simulation methods such as the grand canonical ensemble Monte Carlo (GCMC)[7−10] method and the Gibbs ensemble Monte Carlo (GEMC)[11−14] method have shed light into the physical behavior of confined fluids. However, accurate prediction of the high-pressure adsorption of supercritical gases in carbonaceous materials, based on structural characteristics, is still a challenging task, requiring not only consistency between experimental adsorption measurements and theoretical adsorption models[15] but also rigorous characterization of the carbon internal structure. In practice, slit-pore models have been most commonly used to characterize porous carbons[14,16−19] as well as to predict gas adsorption equilibrium[20−22] on the carbon due to their simplicity, while more complex models[23−26] of the carbon have yet to become routine due to their high computing demand as well as their somewhat specialized nature.

A disadvantage of the slit-pore model, recognized earlier,[14] is that disregard of pore topology may lead to incorrect prediction of the adsorption equilibrium of large molecules using adsorbent characterization obtained from adsorption data of smaller probing molecules. Further, in all adsorption measurements, the determination of excess adsorbed quantities requires adsorbent volume. In practice, the adsorbent volume is normally determined by helium pycnometry. However, the accessibility of helium to the adsorbent surface may be very different from that of the adsorbate molecule due to possible differences in size, shape, and solid−fluid interaction potential strength,

* To whom correspondence should be addressed. E-mail: sureshb@cheque.uq.edu.au.

(1) Nguyen, T. X.; Bhatia, S. K. *Langmuir* **2004**, *20*, 3532.
(2) Nguyen, T. X.; Bhatia, S. K. *J. Phys. Chem. B* **2004**, *108*, *14032*.
(3) Evans, R.; Marconi, U. M. B.; Tarazona, P. *J. Chem. Soc., Faraday Trans.* **1986**, *82*, 1763.
(4) Rosenfeld, Y. *Phys. Rev. Lett.* **1989**, *63*, 980.
(5) Kierlik, E.; Rosingberg, M. L. *Phys. Rev. A* **1991**, *44*, 5025.
(6) Tan, Z.; Gubbins, K. *J. Phys. Chem.* **1992**, *96*, 845.
(7) Norman, G. E.; Filinov, V. S. *High Temp.* **1969**, *7*, 216.
(8) Rowley, L. A.; Nicholson, D.; Parsonage, N. G. *J. Comput. Phys.* **1975**, *17*, 401.
(9) Rowley, L. A.; Nicholson, D.; Parsonage, N. G. *Mol. Phys.* **1976**, *31*, 365.
(10) Adams, D. J. *Mol. Phys.* **1975**, *29*, 307.
(11) Panagiotopoulos, A. Z. *Mol. Phys.* **1987**, *61*, 813.
(12) Panagiotopoulos, A. Z. *Mol. Phys.* **1987**, *62*, 701.
(13) Panagiotopoulos, A. Z.; Quirke, N.; Stapleton, M.; Tildesley, D. J. *Mol. Phys.* **1988**, *63*, 527.
(14) Lastoskie, C.; Gubbins, K. E.; Quirke, N. *J. Phys. Chem.* **1993**, *97*, 4786.
(15) Neimark, A. V.; Ravikovitch, P. I. *Langmuir* **1997**, *13*, 5148.
(16) Bandosz, T. J.; Biggs, M. J.; Gubbins, K. E.; Hattori, Y.; liyama, T.; Kaneko, K.; Pikunic, J.; Thomson, K. T. In *Chemistry and Physics of Carbon*; Radovic, L., Ed.; Marcel Dekker: New York, 2003; Vol. 28, p 41.
(17) Ravikovitch, P. I.; Vishnyakov, A.; Russo, R.; Neimark, A. V. *Langmuir* **2000**, *16*, 2311.
(18) Olivier, J. P. *J. Porous Mater.* **1995**, *2*, 9.
(19) Olivier, J. P. *Carbon* **1998**, *36*, 1469.
(20) Jiang, S.; Zollweg, J. A.; Gubbins, K. E. *J. Phys. Chem.* **1994**, *98*, 5709.
(21) Davies, G. M.; Seaton, N. A. *AIChE J.* **2000**, *46*, 1753.
(22) Davies, G. M.; Seaton, N. A. *Langmuir* **1999**, *15*, 6263.
(23) Segarra, E. I.; Glandt, E. D. *Chem. Eng. Sci.* **1994**, *49*, 2953.
(24) Thomson, K. T.; Gubbins, K. E. *Langmuir* **2000**, *16*, 5761.
(25) Pikunic, J.; Gubbins, K. E.; Pellenq, R. J.-M.; Cohaut, N.; Rannou, I.; Guet, J.-M.; Clinard, C.; Rouzaud, J.-N. *Appl. Surf. Sci.* **2002**, *196*, 98.
(26) Pikunic, J.; Clinard, C.; Cohaut, N.; Gubbins, K. E.; Guet, J.-M.; Pellenq, R. J.-M.; Rannou, I.; Rouzaud, J.-N. *Langmuir* **2003**, *19*, 8565.

10.1021/la047545h CCC: $30.25
Published on Web 02/26/2005

leading to discrepancies between experiments and theoretical predictions.

While disregard of pore topology is undoubtedly a disadvantage of the slit-pore model, observable discrepancies between experiments and theoretical predictions also occur due to other effects. This may arise from poor representation of solid−fluid interactions between adsorbate molecules, especially polar species due to the additional contribution of electrostatic interactions, and the real carbon surface as well as the inherent inconsistency between the experiments and the predictions, as discussed in the above paragraph. In practice, these may obscure errors due to inappropriate topology and affect the capability of the slit-pore model in predicting gas adsorption in carbons. In particular, idealization of the real carbon surface having roughness and crystalline defects by a perfect smooth wall as well as representation of intermolecular interactions by pairwise Lennard-Jones (LJ) interaction through Lorentz combining rules, overlooking multibody interactions, are simplifications that are routinely utilized in the DFT calculations and molecular simulations. These lead to difficulty in determining the proper LJ parameters for fluid−fluid or solid−fluid interactions due to their possible dependence on temperature, density, and even physical and chemical characteristics of the adsorbent surface (defects, functional groups). Such LJ parameters are known to have a significant impact on pore adsorption density.[27] However, this difficulty may be alleviated by the availability of porous carbons on which adsorption measurements of simple gases (Ar, N_2, or CH_4) are well predicted by the slit-pore model. A systematic investigation on the adsorption of these gases on such porous carbons at various temperatures enables one to validate properly the predictive capability of the slit-pore model for gas adsorption as well as to gain important insights into problems of pore network connectivity and the physical behavior of confined fluids under the adsorption force field.

In recent work, we have proposed[1,2] a novel NLDFT-based slit-pore characterization procedure, the finite wall thickness (FWT) model, that enables one to determine simultaneously heterogeneities of pore size and pore wall thickness. Our approach has been applied to determine the pore wall thickness distribution (PWTD) of a series of commercialized activated carbons and coal chars using argon adsorption data at 87 K, with good correspondence with X-ray diffraction. It has been shown to be superior to the infinite wall thickness (IWT) model in interpreting the mechanism of pore generation in porous carbons during the activating process as well as in providing a reliably probed internal structure that enables one to accurately predict adsorption uptake measurements of other gases such as supercritical methane, ethane, and argon at high pressures up to 60 MPa[2]. Following this preliminary success of the FWT model in the prediction of gas adsorption equilibrium, it is important to verify further the consistency of the model by applying it to predict the adsorption of other supercritical gases such as N_2 and CO_2 at various temperatures on different porous carbons. This also permits a better understanding of the pore network connectivity problem, as will be discussed.

2. Theoretical Modeling

2.1. Density Functional Theory. In this work, we use the Tarazona[28,29] NLDFT to calculate the single pore density profile, $\rho(\mathbf{r})$, of the adsorbed phase. The density profile of adsorbate is obtained by minimizing the grand potential, Ω, at fixed temperature, chemical potential, and pore volume in the grand canonical ensemble in the presence of the spatially varying external field, ϕ_{ext}, with

$$\Omega[\rho(\mathbf{r})] = F[\rho(\mathbf{r})] - \int d\mathbf{r}\, [\mu - \phi_{ext}] \quad (1)$$

The intrinsic Helmholtz free energy, $F[\rho(\mathbf{r})]$, is generally determined from a first-order expansion about a reference system of hard spheres of diameter σ_h, under a mean field approximation, leading to

$$F[\rho(\mathbf{r})] = F_h[\rho(\mathbf{r}); \sigma_h] + \frac{1}{2}\int \rho(\mathbf{r})\, d\mathbf{r} \int d\mathbf{r}'\, \rho(\mathbf{r}')\, \phi_{att}(|\mathbf{r} - \mathbf{r}'|) \quad (2)$$

where F_h is the Helmholtz free energy of the hard sphere system and is given as

$$F_h[\rho(\mathbf{r}); \sigma_h] = kT\int d\mathbf{r}\, \rho(\mathbf{r})[\ln(\Lambda^3\rho(\mathbf{r})) - 1] + kT\int d\mathbf{r}\, \rho(\mathbf{r})\, f_{ex}[\bar{\rho}(\mathbf{r}); \sigma_h] \quad (3)$$

Here, $\Lambda = h/(2\pi mkT)^{1/2}$ is the thermal de Broglie wavelength and f_{ex} is the Helmholtz free energy functional per fluid particle, calculated from the Carnahan−Starling equation of state for hard spheres,[30] at a suitably weighted density, $\bar{\rho}(\mathbf{r})$, following

$$\bar{\rho}(\mathbf{r}) = \int \rho(\mathbf{r}')\, \omega(|\mathbf{r} - \mathbf{r}'|, \bar{\rho}(\mathbf{r}))\, d\mathbf{r}' \quad (4)$$

where the weighting function, $\omega(|\mathbf{r} - \mathbf{r}'|, \bar{\rho}(\mathbf{r}))$, is as prescribed by the Tarazona formulation.[29] Here, it is noted that the weighting functions in the original work of Tarazona[28] were incorrect, and it is the subsequently corrected functions[29] that have been employed. The attractive part of the fluid−fluid potential, ϕ_{att}, is determined by the Weeks−Chandler−Andersen (WCA) separation[31] of the fluid−fluid interaction potential, as discussed below.

2.2. Potential Models. The interaction potential between fluid molecules is taken as the Lennard-Jones (LJ) 12-6 potential

$$\phi_{ff}(r) = 4\epsilon_{ff}\left[\left(\frac{\sigma_{ff}}{r}\right)^{12} - \left(\frac{\sigma_{ff}}{r}\right)^{6}\right] \quad (5)$$

where r is the interparticle distance, σ_{ff} is the collision diameter, and ϵ_{ff} is the well depth. Following the WCA separation,[31] the attractive part of this potential is represented as

$$\phi_{ff}(|\mathbf{r} - \mathbf{r}'|) = \phi_{ff}(|\mathbf{r} - \mathbf{r}'|) \qquad |\mathbf{r} - \mathbf{r}'| > r_m$$
$$= -\epsilon_{ff} \qquad |\mathbf{r} - \mathbf{r}'| < r_m \quad (6)$$

where $r_m = 2^{1/6}\sigma_{ff}$. The interaction potential, $\phi_{wf}(z)$, between a carbon wall and an adsorbate molecule is represented by[32]

(27) Yin, Y. F.; McEnaney, B.; Mays, T. J. *Carbon* **1998**, *36*, 1425.
(28) Tarazona, P. *Phys. Rev.* A **1985**, *31*, 2672; **1985**, *32*, 3148.
(29) Tarazona, P.; Marini, B. M., U.; Evans, R. *Mol. Phys.* **1987**, *60*, 573.
(30) Carnahan, N. F.; Starling, K. E. *J. Chem. Phys.* **1969**, *51*, 635.
(31) Weeks, J. D.; Chandler, D.; Andersen, H. C. *J. Chem. Phys.* **1971**, *54*, 5237.
(32) Steele, W. A. *Surf. Sci.* **1973**, *36*, 317.

$$\phi_{wf}(z, n) = 2\pi\rho_c\sigma_{cf}^2 \epsilon_{cf}\sum_{i=0}^{n-1}\left[\frac{2}{5}\left(\frac{\sigma_{cf}}{z + i\Delta}\right)^{10} - \left(\frac{\sigma_{cf}}{z + i\Delta}\right)^{4}\right], z > 0 \quad (7)$$

Here, z is the (center to center) distance between the fluid molecule and the pore wall surface, n is the number of graphene layers in the pore wall, Δ is the interlayer spacing, and ρ_c is the number of carbon atoms per unit area in a single graphene layer. Following Steele,[32] the parameters $\Delta = 3.35$ nm and $\rho_c = 0.3817$ atoms·Å^{-2}, corresponding to graphite, are used.

The asymmetric external potential profile, $\phi_{ext}(z, l, m)$, for a slit-shaped pore having pore size H is determined from superposition of the potentials of the opposing pore walls

$$\phi_{ext}(z, l, m) = \phi_{wf}(z, l) + \phi_{wf}(H - z, m) \quad (8)$$

where l and m are the arbitrary numbers of graphene layers in the two opposing walls.

2.3. Adsorption Model. We use the general adsorption isotherm (GAI), whereby the excess adsorbed amount, $\Gamma_{ex}(P)$, is given as

$$\Gamma_{ex}(P) = \int[\hat{\rho}(P, H_{in}) - \rho_b]f(H_{in})\, dH_{in} \quad (9)$$

where $f(H_{in})$ is the pore size distribution (PSD) of the adsorbent, $H_{in} = (H_{cc} - \sigma_c)$ is the geometrical pore width, H_{cc} is the physical pore width, σ_c is the effective diameter of the carbon atom, and ρ_b is the bulk density. $\hat{\rho}(P, H_{in})$ is the average density in a pore of width H_{in} at a given pressure, P. The definition of the average density is dependent upon the pore model used. For the finite wall thickness (FWT) model considered here, in which the adsorbate−wall potential is represented by eq 7, the average density is defined as[33]

$$\hat{\rho}(P, H_{in}) = \sum_{m=1}^{\infty}p(m)\sum_{l=1}^{\infty}\rho(l)\frac{1}{H_{in}}\int_0^{H_{cc}}\rho_{lm}(P, H_{in}, z)\, dz \quad (10)$$

where $p(n)$ is a wall thickness probability distribution and $\rho_{lm}(P, H_{in}, z)$ is the local density profile in a pore of geometrical width H_{in}, with the left wall having l graphene layers and the right wall having m layers, obtained from the NLDFT. Here, we assume that the thicknesses of the two opposing walls of a pore are uncorrelated and that the interaction potential between adsorbed molecules in neighboring pores is insignificant in comparison to the fluid−solid potential energy, justified by the recent study from this laboratory[33] showing the former to have a negligible effect on the isotherm for small molecules such as nitrogen.

2.4. Simultaneous Determination of Pore Size and Pore Wall Thickness Distributions. Earlier attempts at characterization considering finite pore walls have been largely ad hoc, utilizing arbitrary assumptions regarding the thicknesses of the confining walls, for instance, that one wall is infinitely thick while the other has exactly one graphene layer.[34] Such assumptions have resulted in unrealistic surface areas and have therefore not led to a viable solution. Our use of the probability distribution, $p(n)$, eliminates such arbitrary assumptions.

In practice, the interaction potential energy is insensitive to the stacking number, n, for thick walls having five or more carbon layers. Consequently, we lump the combined probability for all the thick walls having five or more carbon layers into $p(4+)$. The pore wall thickness distribution, $\mathbf{p} = \{p(n); n = 1, 2, 3, 4, 4+\}$, and the pore size distribution, $f(H_{in})$, can then be solved simultaneously by minimizing the deviation, δ, between the theoretically estimated adsorbed quantity, Γ_{ex}, and the corresponding experimental quantity, $C_{exp}(P)$, where

$$\delta = ||\Gamma_{ex} - C_{exp}||^2 \quad (11)$$

with Γ_{ex} given by eqs 9 and 10. Minimization of δ following eq 11 is subjected to the following constraints

$$\sum_{n=1}^{4+}p(n) = 1 \qquad \sum_{n=1}^{4}np(n) + 5p(4+) \le \gamma \quad (12)$$

and the mean number of graphene sheets in a pore wall, γ, is given as[1,2,33]

$$\gamma = \frac{2630(1 - w_a)}{S_g} \quad (13)$$

Here, w_a is the mass fraction of ash content in the carbon and S_g is the surface area of the adsorbent given by

$$S_g = \int_0^{\infty}\frac{2}{H_{in}}f(H_{in})\, dH_{in} \quad (14)$$

Minimization of δ subjected to the constraints in eqs 12 and 13 is performed using a genetic algorithm,[35] coupled with Tikhonov regularization.[36] The L-curve technique[37] is used for determining the regularization parameter. In particular, we employ the PSD obtained using the above procedure as the guessed PSD, f_{guess}, with the infinitely thick wall model used to determine the smoothing parameter. The guessed pore wall thickness distribution, $\mathbf{p}_{guess}$, is then determined using eqs 13 and 14 together with an appropriate statistical distribution.[38] The solution space in the vicinity of the guessed solution (f_{guess}, $\mathbf{p}_{guess}$) can then be generated using the constraints given in eq 12. Subsequently, the solution of the PSD and PWTD is searched in this space. The final solution of the PSD and PWTD is obtained after a few iterations of the above procedure using the genetic algorithm,[35] in which the guessed solution (f_{guess}, $\mathbf{p}_{guess}$) for the next iteration is taken from the result of the previous iteration.

3. Grand Canonical Monte Carlo Simulations

Grand Canonical Monte Carlo (GCMC) simulation is a commonly used technique to study the adsorption of confined fluids as well as the properties of bulk fluids, especially under supercritical conditions. In GCMC simulation, the chemical potential, μ, volume, V, and temperature, T, are kept invariant, while the number of particles, N, and associated configurational energy, E, are allowed to fluctuate. In the simulation, the generation of microstate configuration was fulfilled by the adoption of a well-established Metropolis sampling scheme for three trial

(33) Bhatia, S. K. *Langmuir* **2002**, *18*, 6845.
(34) Ravikovitch, P. I.; Jagiello, J.; Tolles, D.; Neimark, A. V. Carbon '01, International Conference on Carbon (Lexington, 2001).
(35) Zbigniew., M. *Genetic algorithms + data structures = evolution programs*, 3rd ed.; Springer-Verlag: New York, 1996.
(36) Tikhonov, A. N. *Dokl. Akad. Nauk SSSR* **1963**, *153*, *49*.
(37) Hansen, P. C. *Nord. Tidskr. Informations Behandling* **1990**, *30*, 658.
(38) Consul, P. C. *Generalized Poisson distributions: Properties and Applications*; Marcel Dekker: New York, 1989.

Table 1. Lennard-Jones Parameters for Fluid−Fluid Interaction of Argon, Nitrogen, Methane, and Carbon Dioxide

gas	σ_{ff} (Å)	ϵ_{ff}/k_B (K)	source
	NLDFT Calculations		
Ar	3.2124	113.97	43
N_2	3.4764	98.07	43
CH_4	3.6177	223.35	43
CO_2	3.472	221.98	present work
	GCMC Simulations		
Ar	3.40	119.0	present work
N_2	3.655	93.98	present work
CH_4	3.751	148.0	present work
CO_2	C: 2.824	C: 28.68	present work
	O: 3.026	O: 82.0	
l_{oo}(Å)	O−O: 2.324		
l_q(e)	C: 0.664		
	O: 0.332		

types: moving (including rotation for nonspherical molecules such as carbon dioxide and ethane), creating, and deleting molecules. Accordingly, the probability of these three trial types being accepted is given by Adams' algorithm.[39]

In the current work, the GCMC simulations have been carried out to validate the calculations of pore adsorption isotherms, obtained from nonlocal density functional theory (NLDFT). In the adsorption simulation, a simple molecule such as argon, nitrogen, or methane is modeled as one LJ center molecule. The LJ potential is truncated at 15 Å. The LJ parameters for fluid−fluid interaction are obtained from the fit of the LJ equation of state of Johnson et al.[40] to the experimental bulk data, reproduced accurately by the Bender equation of state.[41] The LJ parameters of these gases are given in Table 1. Periodic boundary conditions were applied to directions parallel to the walls. The size of the primary simulation cell, quadratic in the plane parallel to the walls, is 70×70 Å^2. The number of the configurations for each molecule is about 3×10^6.

For a more complex molecule such as carbon dioxide, the results of pore density profile obtained from NLDFT calculations are validated against the GCMC simulated results employing a molecular model of carbon dioxide, taken from Hammonds et al.,[42] based on the three-center (LJ) approximation with partial charges at each site. Suitable adjustment of the LJ parameters for fluid−fluid interactions that reproduce the experimental bulk data of carbon dioxide was made. In bulk and adsorbed phase GCMC simulations, the LJ potential is truncated at 20 Å. No long-range correction was employed.[43] The number of configurations ranges from 1.5×10^7 to 2.0×10^7. For the bulk simulation, the primary simulation cell is cubic and has a size of $50 \times 50 \times 50$ Å^3. Periodic boundary conditions were imposed. For the adsorption simulation, the conditions of primary simulation cells are assigned as described for argon, nitrogen, and methane in the above section. The interaction potential between a carbon wall and an adsorbate molecule, described in eq 7, is applied and the Lorentz−Berthelot combining rules have been utilized for the determination of LJ parameters for solid−fluid interactions.

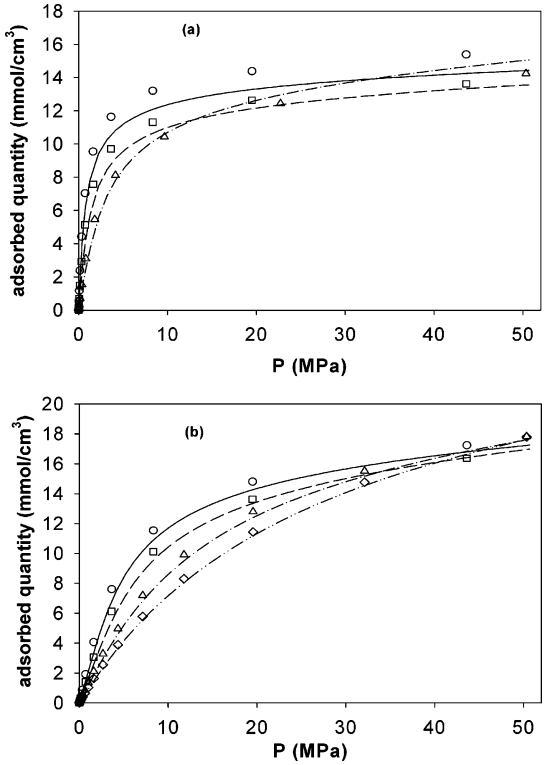

Figure 1. Comparison between GCMC simulated and DFT calculated adsorption isotherms of supercritical argon at 298 K in various slit-pore sizes. The pore walls contain a single carbon plane. The open symbols depict the GCMC simulated isotherms, and the lines represent the corresponding DFT calculated isotherms. The pore widths are as follows: (a) circles and solid line, 3.51 Å; squares and dashed line, 4.44 Å; triangles and dashed−dotted line, 5.60 Å. (b) circles and solid line, 7.06 Å; squares and dashed line, 8.90 Å; triangles and dashed−dotted line, 14.14 Å; diamonds and dashed−dotted−dotted line, 22.44 Å.

4. Results and Discussion

4.1. Comparison of Adsorption Isotherms Obtained from GCMC Simulation and DFT. Before comparison with experimental data in this section, results of isotherms of several investigated gases (Ar, N_2, CH_4, and CO_2) at various pore sizes, calculated using the DFT approach, are validated against the corresponding simulated results. The validation conducted covers the pore size range of the pore size distribution of the investigated carbons and is presented in the following sections.

4.1.1. Methane, Argon, and Nitrogen. To compare faithfully with the GCMC simulated results, the DFT-based adsorption modeling should employ the same LJ parameters as those used in the GCMC simulation. However, this may lead to significant deviations for even the simplest systems due to the fact that the GCMC and DFT approaches do not yield the same equation of state.[44] This is due to the mean field nature of the DFT and the associated WCA[31] splitting of the potential. Accordingly, we adopt the Ravikovitch et al. approach[44] that obtains the LJ parameters for fluid−fluid interactions utilized in NLDFT calculations of pore adsorption isotherms so that the DFT equation of state reproduces experimental bulk data. For simple gases such as CH_4, Ar, and N_2, the parameters are taken from work done by Ustinov et al.[45] who determined the parameters from the fit of the DFT

(39) Adams, D. J. *Mol. Phys.* **1975**, *29*, 311.
(40) Johnson, J. K.; Zollweg, J. A.; Gubbins, K. E. *Mol. Phys.* **1993**, *78*, 591.
(41) Bender, E. *Proceedings of the Fifth Symposium on Thermophysical Properties*; ASME, 1970; p 227.
(42) Hammonds, K. D.; McDonald, I. R.; Tildesley, D. J. *Mol. Phys.* **1993**, *78*, 173.
(43) Cracknell, R. F.; Nicholson, D.; Tennison, S. R. R.; Bromhead, J. *Adsorption* **1996**, *2*, 193.
(44) Ravikovitch, P. I.; Vishnyakov, A.; Neimark, A. V. *Phys. Rev. E* **2001**, *64*, 011602.
(45) Ustinov, E. A.; Do, D. D. *Langmuir* **2003**, *19*, 8349.

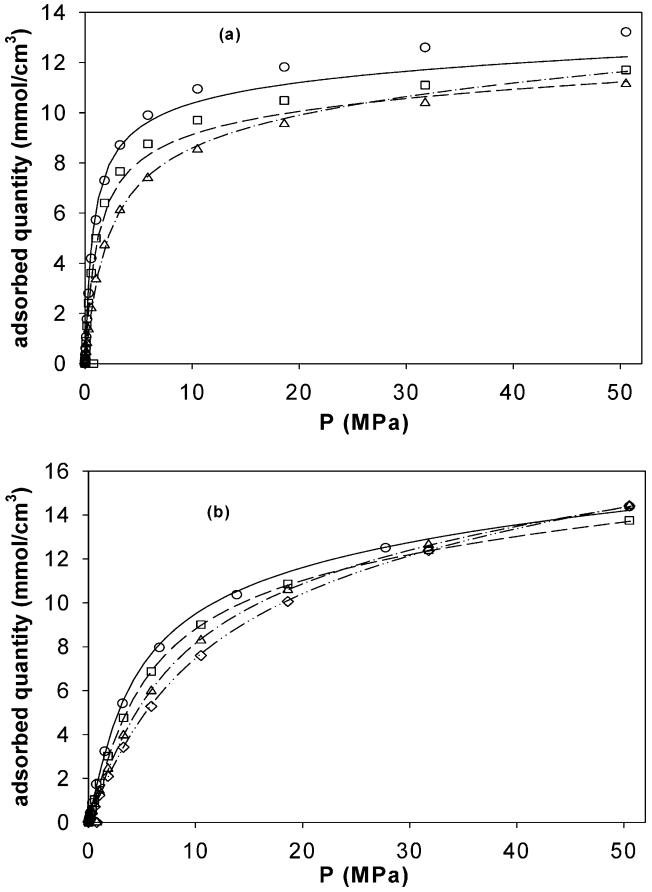

Figure 2. Comparison between GCMC simulated and DFT calculated adsorption isotherms of supercritical nitrogen at 298 K in various slit-pore sizes. The pore walls contain a single carbon plane. The open symbols depict the GCMC simulated isotherms, and the lines represent the corresponding DFT calculated isotherms. The pore widths are as follows: (a) circles and solid line, 3.51 Å; squares and dashed line, 4.65 Å; triangles and dashed−dotted line, 5.60 Å. (b) circles and solid line, 7.06 Å; squares and dashed line, 8.90 Å; triangles and dashed−dotted line, 11.22 Å; diamonds and dashed−dotted−dotted line, 14.14 Å.

equation of state to experimental data at 293 K. The LJ parameters for wall−fluid interactions utilized for both the DFT and GCMC simulations are determined by the Lorentz−Berthelot combining rules, using the values ϵ_c/k = 28 K and σ_c = 3.4 Å for carbon−carbon interaction in graphite.[32]

Figures 1, 2, and 3 depict the comparisons between isotherms of Ar, N_2, and CH_4, respectively, at 298 K from the NLDFT calculations and the corresponding GCMC simulated results, for various pore sizes. From these figures, it is observed that the isotherms of these three gases, calculated by the NLDFT approach, match very well the corresponding simulation results up to 50 MPa in relatively large pores (H_{in} > 3.51 Å). In the small pores (H_{in} ≤ 3.51 Å), the adsorbed phase density determined from the DFT approach slightly underpredicts that obtained from the GCMC simulation at relatively high pressures (>7 MPa). Such an overestimation is normally recognized as a consequence of the mean field approximation. Fortunately, these small pores are absent in the pore size distribution of the BPL and Norit R1 extra carbons, obtained using argon adsorption and the FWT model,[2] while they form a relatively significant proportion in the PSD results obtained using the IWT model for these carbons. Accordingly, the DFT approach can replace the GCMC simulation technique, which requires substantially

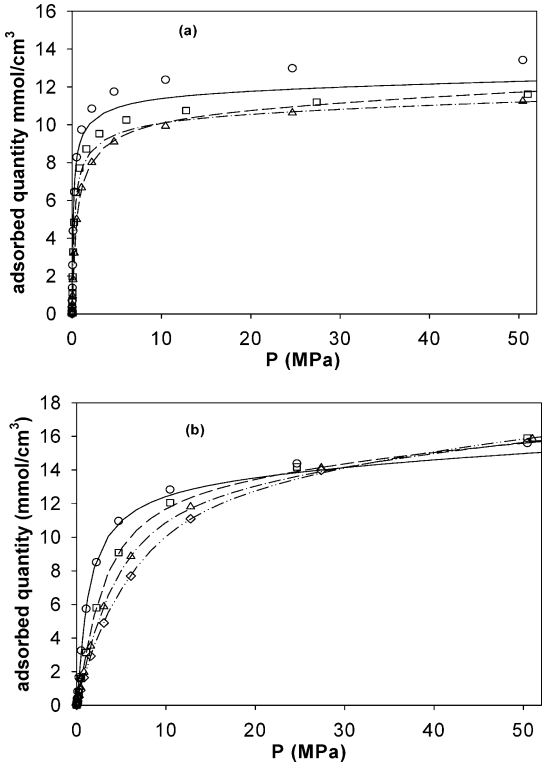

Figure 3. Comparison between GCMC simulated and DFT calculated adsorption isotherms of supercritical methane at 298 K in various slit-pore sizes. The pore walls contain a single carbon plane. The open symbols depict the GCMC simulated isotherms, and the lines represent the corresponding DFT calculated isotherms. The pore widths are as follows: (a) circles and solid line, 3.51 Å; squares and dashed line, 4.87 Å; triangles and dashed−dotted line, 5.60 Å. (b) circles and solid line, 6.47 Å; squares and dashed line, 11.20 Å; triangles and dashed−dotted line, 14.14 Å; diamonds and dashed−dotted−dotted line, 17.82 Å.

more computation, to predict the adsorption equilibrium of the gases in the BPL and Norit R1 extra carbons with good accuracy if the FWT model is utilized.

4.1.2. Carbon Dioxide. Carbon dioxide is a polar and nonspherical molecule. Accordingly, an effective LJ representation of the molecule utilized for NLDFT calculations may not properly capture important physical behavior of its adsorbed phase. However, Vishnyakov et al.[46] showed that pore adsorption isotherms of carbon dioxide at 273 K from NLDFT calculations using one effective LJ center are in satisfactory agreement with the GCMC simulated results using the three-LJ-center model. Further, Ravikovitch et al.[17] achieved good agreement between NLDFT-based PSD results using an effective LJ representation of CO_2 and the GCMC-simulation-based PSD using the three-LJ-center model of this molecule. This also provides motivation to investigate the capability of the NLDFT approach to predict the high-pressure adsorption of supercritical carbon dioxide.

In a manner similar to the previous section, LJ parameters for the fluid−fluid interactions of the carbon dioxide molecule utilized for the NLDFT calculations were determined from the fit of the DFT equation of state to the experimental bulk data at 343 K, generated accurately by the Span−Wagner equation of state.[47] The parameters are reproduced in Table 1. LJ parameters for wall−fluid interactions utilized for both the DFT and GCMC simula-

(46) Vishnyakov, A.; Ravikovitch, P. I.; Neimark, A. V. *Langmuir* **1999**, *15*, 8736.
(47) Span, R.; Wagner, W. *J. Phys. Chem. Ref. Data* **1996**, *25*, 1509.

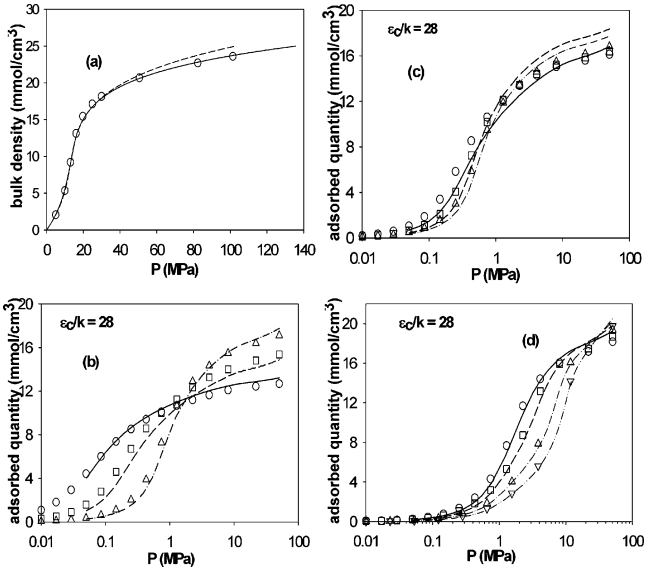

Figure 4. (a) Bulk isotherms of carbon dioxide obtained from the DFT equation of state (dashed line), GCMC simulation (open circles), and the Span and Wagner equation of state[47] (solid line), respectively. (b–d) Comparison between GCMC simulated and DFT calculated adsorption isotherms of supercritical carbon dioxide at 343 K in various slit-pore sizes. Infinite pore wall thickness is assumed. The open symbols depict the GCMC simulated isotherms, and the lines represent the corresponding DFT calculated isotherms. The pore widths are as follows: (b) circles and solid line, 4.44 Å; squares and dashed line, 5.60 Å; triangles and dashed–dotted line, 8.90 Å. (c) circles and solid line, 6.14 Å; squares and dashed line, 7.06 Å; triangles and dashed–dotted line, 7.75 Å. (d) circles and solid line, 11.22 Å; squares and dashed line, 14.14 Å; up-triangles and dashed–dotted line, 22.44 Å; down-triangles and dashed–dotted–dotted line, 35.61.

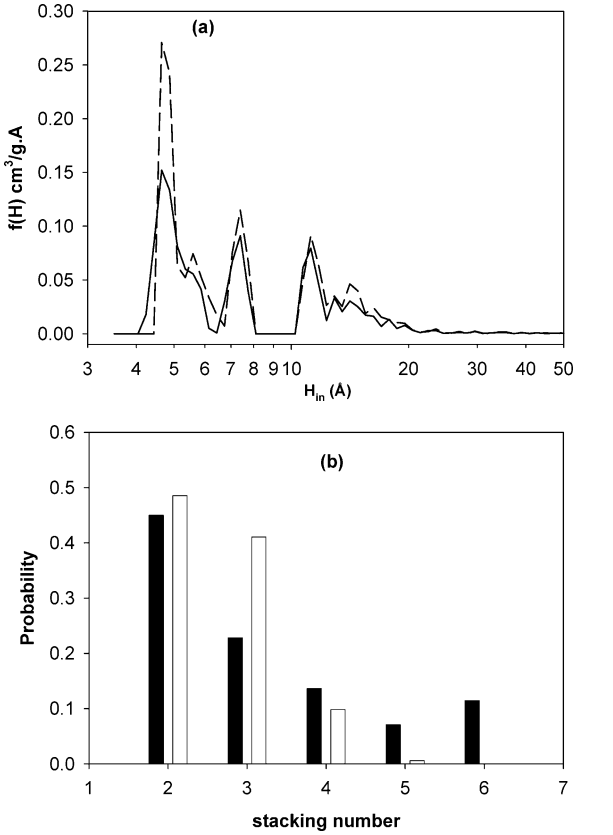

Figure 5. (a) Pore size distribution of BPL (solid line) and Norit R1 extra (dashed line) carbons. (b) Pore wall thickness distribution results of the BPL (filled bars) and Norit R1 extra (open bars) carbons. The PSD and PWTD results were determined by interpretation of argon adsorption at 87 K using the FWT model.

tion were determined by the Lorentz–Berthelot combining rules applied to each LJ site of the fluid, using the values $\epsilon_c/k = 28$ K and $\sigma_c = 3.4$ Å for carbon–carbon interaction in graphite.[32] Figure 4a depicts the comparison between bulk isotherms obtained from the DFT equation of state (dashed line) and the GCMC simulated results (open circles), using LJ parameters presented in Table 1, with the experimental bulk data at 343 K. From the figure, it can be seen that the DFT equation of state provides a reasonable fit to the experimental data up to 20 mmol/cm^3 with a small deviation at high densities (>20 mmol/cm^3), while the bulk isotherm predicted by the GCMC simulation has excellent agreement with the experimental bulk data over the whole range.

Figure 4b–d illustrates comparisons between the results of single pore isotherms from the NLDFT calculations (lines) and those obtained from the GCMC simulations (symbols), demonstrating good agreement for small pores ($H_{in} = 4.4363–8.9032$ Å), as seen in Figure 4b, as well as large pores ($H_{in} \geq 11.222$ Å), as seen in Figure 4d. In Figure 4c, the isotherms in the pores ($H_{in} = 6.14–7.74$ Å) from the NLDFT calculations show a maximum deviation of 10% from the corresponding GCMC simulated results at relatively high pressures (>1MPa), especially for the pore of width $H_{in} = 7.06$ Å, similar to the results of Vishnyakov et al.[46] at a similar pore size. This observation can be explained by lesser efficient packing of the three-LJ-center-modeled molecules than the corresponding spherical ones in the pore size range.[48] However, theoretical adsorption isotherms on the BPL and Norit R1 extra carbons, predicted using pore adsorption isotherms from the NLDFT calculations through eq 9, may have only a small deviation in comparison with those determined from the GCMC simulated pore isotherms due to a very small population of such pores in the PSD results of these examined carbons.

4.2. Prediction of the High-Pressure Adsorption of Supercritical Gases. *4.2.1. Methane.* In our recent paper,[2] we showed that the FWT model provides an accurate prediction of the adsorption measurements[49] of supercritical methane in BPL activated carbon at 298 K up to 60 MPa and is more realistic than the conventional infinite wall thickness approach. The current work is aimed at further applying the FWT model to predict the adsorption of this gas on different carbons at various temperatures. All the predicted adsorption isotherms in the BPL and Norit R1 extra carbons, discussed in later sections, are generated by the FWT model, using characterization results of the examined carbons[2] reproduced in Figure 5.

Figure 6 presents comparisons between the adsorption isotherms on the BPL carbon, predicted by the FWT model (lines) and the corresponding experimental adsorption data at two different temperatures (283 and 303 K). The experimental measurements, determined by the volumetric method, are taken from Belmabkout et al.[50] As seen in the figure, the predictions by the FWT model are in excellent agreement with the corresponding adsorption

(48) Bhatia, S. K.; Tran, K.; Nguyen, T. X.; Nicholson, D. *Langmuir* **2004**, *20*, 9612

(49) Vidal, D.; Malbrunot, L.; Guengant, L.; Vermesse, J. *Rev. Sci. Instrum.* **1990**, *61*, 1314.

(50) Belmabkhout, Y.; De Weireld, G.; Frere, M. *J. Chem. Eng. Data* **2004**, *49*, *1379*.

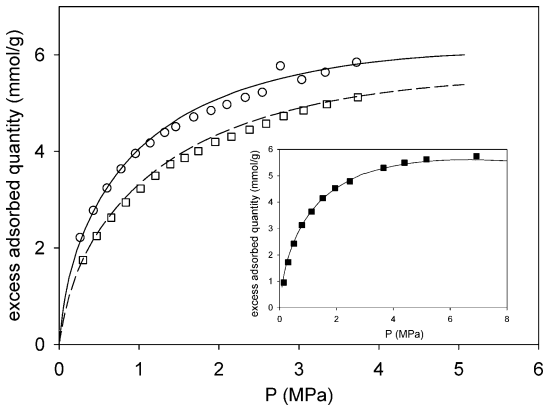

Figure 6. Predicted (lines) and experimental (symbols) adsorption isotherms of supercritical methane on BPL carbon at various temperatures. The solid line and dashed line depict the predicted isotherms at 283 and 303 K, respectively, obtained from the FWT model using the solid interaction parameter ϵ_o/k = 28. The open symbols depict experimental data at 283 K (circles) and 303 K (squares), taken from Belmabkhout et al.[50] In the inset, the solid line depicts the predicted isotherm at 298 K using the FWT model and the filled squares represent the experimental data at 298 K, taken from Quinn.[51]

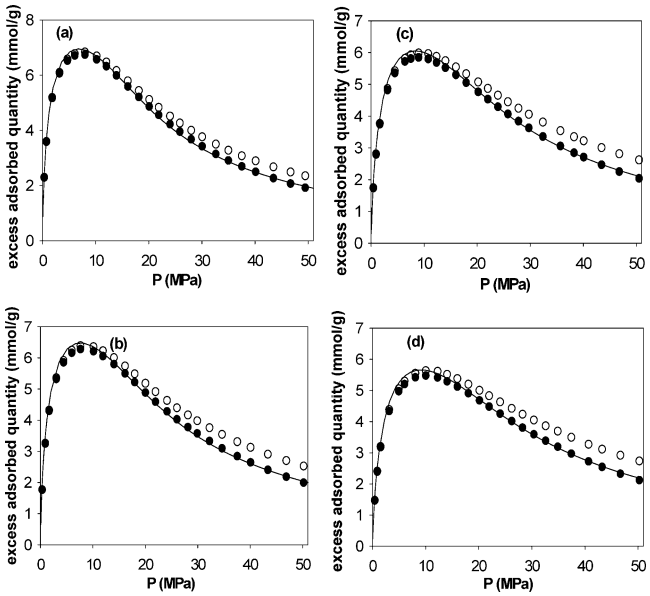

Figure 7. Predicted and experimental adsorption isotherms of supercritical methane on Norit R1 extra carbon at various temperatures. The solid lines depict the predicted isotherms obtained from the FWT model using the solid interaction parameter $\epsilon_o/k = 28$. The open circles depict experimental data taken from Herbst and Harting,[52] and the filled circles are recalculated experimental data using the new carbon volume, V_c, 0.436 cm^3/g: (a) 298 K; (b) 313 K; (c) 328 K; (d) 343 K.

measurements within the experimental error within a maximum of 6%.[50] Furthermore, it is noted that the model also predicts properly methane adsorption data in the BPL carbon at 298 K, taken from Quinn,[51] as shown in the inset of Figure 6.

Parts a−d of Figure 7 illustrate a comparison between theoretical adsorption isotherms on the Norit R1 extra activated carbon at four different temperatures (298, 313, 328, and 343 K, respectively) up to 50 MPa, calculated by the FWT model (solid line), and experimental adsorption data (open circles) taken from Herbst and Harting.[52] It is observed that the FWT model predicts the experimental

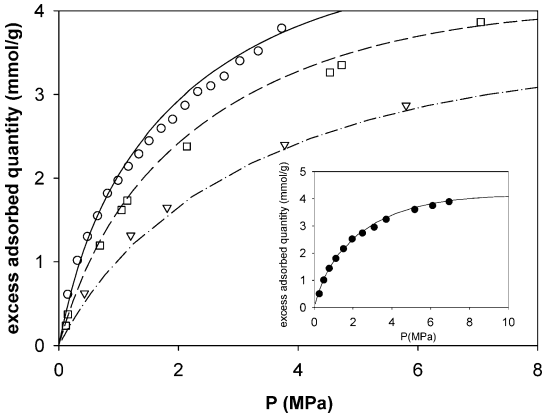

Figure 8. Predicted and experimental adsorption isotherms of supercritical nitrogen on BPL carbon at various temperatures. The solid, dashed, and dashed−dotted lines depict the predicted isotherms at 283, 303, and 343 K, respectively, obtained from the FWT model using the solid interaction parameter $\epsilon_o/k = 28$. The open symbols depict experimental data at 283 K (circles) taken from Belmabkhout et al.[50] and at 303 K (squares) and 343 K (down triangles) taken from Sircar.[57] In the inset, the solid line depicts the adsorption prediction and the filled circles represent the experimental data at 298 K taken from Quinn.[51]

adsorption data (open circles) consistently in the low-pressure region (<10 MPa). However, the predicted isotherms from the model increasingly deviate from the experimental data with increasing pressure in the high-pressure region (>10MPa). This deviation increases with increasing temperature. This is due to inaccurate determination of the adsorbent volume, utilized for calculating the experimental data by the gravimetric method, when assuming nonadsorbable helium.[53] Although such inaccuracy can be expected to be small, it may lead to significant error of excess adsorbed quantity in the high-pressure region where the bulk phase is dense.

To correct the above error, in the calculations behind Figure 7, for consistency between the experiments and the predictions, we used the FWT-based theoretically calculated adsorption isotherm of methane at 298 K to determine the adsorbent volume from the experimental data at this temperature. The adsorbent volume had previously been fitted as a function of temperature by Herbst and Harting,[52] but this was found unsatisfactory using our more rigorous DFT-based approach. The fitting task is based on the equation employed by Herbst and Harting[52] to calculate the experimental specific excess adsorption, C_{exp}, following

$$C_{exp} = \frac{\Omega + \rho_f V_c}{m} \tag{15}$$

where V_c is the adsorbent volume, m is the carbon sample weight, and Ω is the reduced mass, given by

$$\Omega = m^s + \rho_f V_{cont} \tag{16}$$

Here, m^s is the microbalance signal, ρ_f is the bulk fluid density, and V_{cont} is the volume of the sample container. In eq 15, the adsorbent volume, V_c, is considered as a unique temperature-independent fitting parameter in the current work. We obtain the new value of the adsorbent volume ($V_c = 0.436$ cm^3/g) that offers excellent agreement between the experiment and prediction at 298 K, as seen in Figure 7a. Subsequently, we employed the new adsorbent volume to recalculate the other experimental

(51) Quinn, D. F. *Carbon* **2002**, *40*, 2767.
(52) Herbst, A.; Harting, P. *Adsorption* **2002**, *8*, 111.
(53) Malbrunot, P.; Vidal, D.; Vermesse, *J. Langmuir* **1997**, *13*, 539.

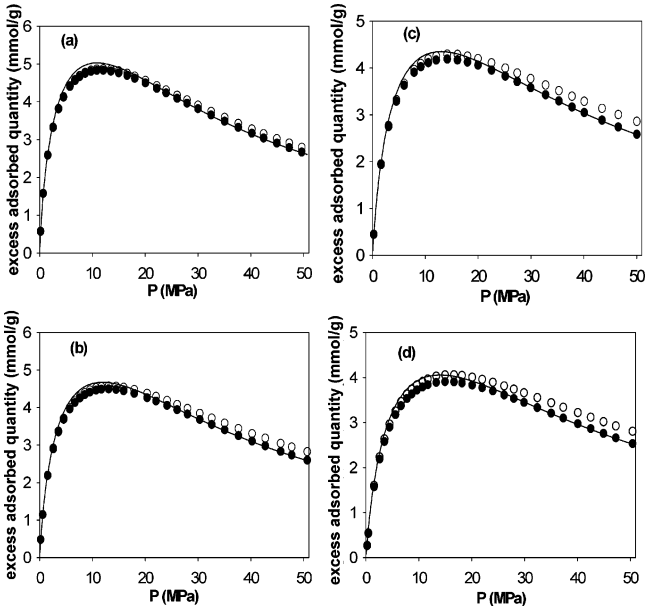

Figure 9. Predicted and experimental adsorption isotherms of supercritical nitrogen on Norit R1 extra carbon at various temperatures. The solid line depicts the predicted isotherms obtained from the FWT model using the solid interaction parameter $\epsilon_c/k = 28$. The open circles depict experimental data taken from Herbst and Harting,[52] and the filled circles are recalculated experimental data using the new carbon volume, V_c, 0.453 cm^3/g.

excess adsorption isotherms at 313, 328, and 343 K using eq 15. All the recalculated experimental adsorption isotherms are given (represented by filled circles) in Figure 7b−d. From these figures, it can be seen that the predicted adsorption isotherms produced by the FWT model match very well all the recalculated adsorption isotherms at the three investigated temperatures (313, 328, and 343 K), supporting the use of a constant value of the adsorbent volume in the temperature range 298−343 K. This is consistent with a low thermal expansion coefficient of carbon[54] but contradicts significant temperature dependence of the adsorbent volume[49] determined by means of buoyancy measurements with helium with nonadsorbable helium assumption.

4.2.2. Nitrogen. The adsorption of nitrogen at 77 K is most commonly used to characterize porous materials. Although nitrogen is inherently nonspherical and weakly polar, spherical nitrogen models have been widely adopted[14,17,55] in DFT calculations that are much faster than molecular simulation, leading to feasibility of developing DFT-based characterization methods for porous materials having a wide pore size range. On the other hand, more realistic nitrogen models,[43,56] involving two LJ centers with partial charges located along the molecular axis, have also been investigated. In the current approach, the spherical nitrogen model was adopted in our DFT calculations to generate isotherms, as discussed earlier in section 4.1.1.

Figure 8 and its inset show a comparison of the adsorption isotherms of supercritical nitrogen in BPL carbon at four different temperatures (283, 298, 303, and 343 K). The lines represent the adsorption isotherms, predicted by the FWT model. Further, the open circles depict experimental adsorption data at 283 K, taken from

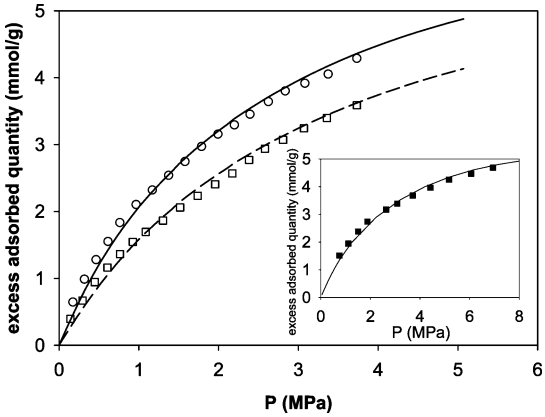

Figure 10. Predicted and experimental adsorption isotherms of supercritical argon on BPL carbon at various temperatures. The solid and dashed lines depict the predicted isotherms at 283 and 303 K, respectively, obtained from the FWT model using the solid interaction parameter $\epsilon_c/k = 28$. The open symbols depict experimental data at 283 K (circles) and at 303 K (squares) taken from Belmabkhout et al.[50] In the inset, the solid line depicts the predicted isotherm by the FWT model and the filled circles represent the experimental data at 298 K taken from Quinn.[51]

Belmabkhout et al.;[50] the open squares and triangles represent those at 303 and 343 K, respectively, taken from Sircar;[57] and the filled circles represent those at 298 K, taken from Quinn et al.[51] It is evident that the isotherms predicted by the FWT model have good agreement with the experimental adsorption data at all the examined temperatures.

Parts a−d of Figure 9 show comparisons between the theoretically predicted FWT model isotherms (solid lines) in Norit R1 extra activated carbon and the corresponding experimental results (open circles) at 298, 313, 328, and 343 K, respectively, up to 50 MPa. The experimental results, measured by the gravimetric technique, are taken from Herbst and Harting.[52] In these figures, similar results to those of methane adsorbed on the same carbon, as shown earlier in section 4.2.1, are also observed for nitrogen. In particular, the theoretically predicted isotherms match very well the experimental results at all the examined temperatures in the low-pressure range (<20 MPa) with a slight deviation from the experimental results with increasing temperature in the higher pressure range, as seen in Figure 9. This is due to reasons similar to those explained in an earlier section for methane adsorption in the same carbon. As in the case of methane adsorption, the nitrogen adsorption data were corrected by using eq 15 to fit the adsorbent volume. The corrected experimental results (filled circles) using the new adsorbent volume (V_c = 0.453 cm^3/g) are depicted in Figure 9. From this figure, excellent agreement between the theoretically predicted isotherms and the recalculated experimental results is apparent. At this point and in the following sections, it can be seen that the new adsorbent volume determined for nitrogen is slightly higher than that of methane, which is consistent with the different accessibility to the carbon surface to these adsorbates.[45]

4.2.3. Argon. Similar results to those for methane and nitrogen, illustrated in the above sections, are also observed for argon. Figures 10 (argon adsorption on the BPL carbon) and 11 (argon adsorption in Norit R1 extra carbon) demonstrate excellent agreement between the experimental data and the theoretically predicted isotherms made using the FWT model (solid lines). Interest-

(54) Gumma, S.; Talu, O. *Adsorption* **2003**, *9*, 17.
(55) Jagiello, J.; Thommes, M. *Carbon* **2004**, *42*, 1225.
(56) Kaneko, K.; Cracknell, R. F.; Nicholson, D. *Langmuir* **1994**, *10*, 4606.
(57) Sircar, S. *J. Chem. Soc., Faraday Trans. 1* **1984**, *80*, 1101.

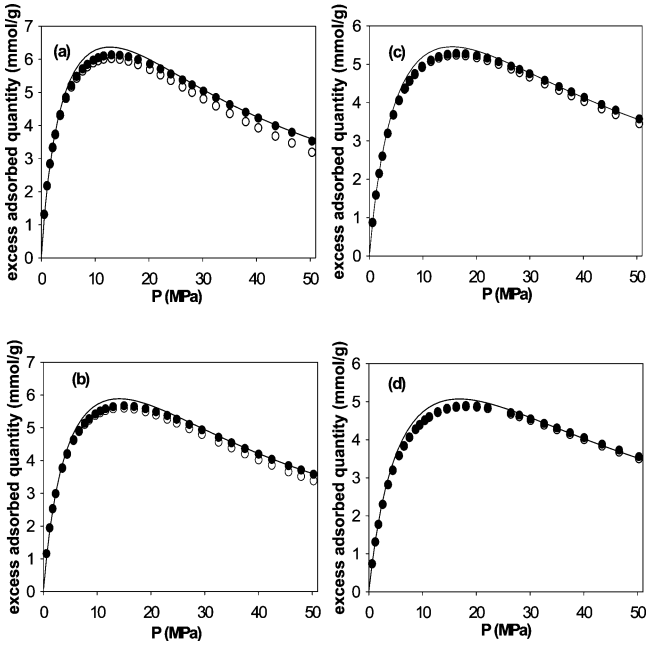

Figure 11. Predicted and experimental adsorption isotherms of supercritical argon on Norit R1 extra carbon at various temperatures. The solid line depicts the predicted isotherm obtained from the FWT model model using the solid interaction parameter $\epsilon_c/k = 28$. The open circles depict experimental data taken from Herbst and Harting,[52] and the filled circles are recalculated experimental data using the carbon volume, V_c, 0.481 cm^3/g: (a) 298 K; (b) 313 K; (c) 328 K; (d) 343 K.

ingly, the new adsorbent volume (V_c = 0.481 cm^3/g), calculated by a similar treatment to that for methane and nitrogen, approaches that determined by helium pycnometry assuming nonadsorbable helium assumption at the highest temperature (343 K) (V_c = 0.477 68 cm^3/g, taken from Herbst and Harting[52]). This indicates that the nonadsorbable helium assumption may only be valid at high temperatures at which helium adsorption is negligible. This is confirmed by the work of Malbrunot et al.,[53] who showed negligible helium adsorption at 400 °C at atmospheric pressure.

4.2.4. Carbon Dioxide. In section 4.1.2, we showed satisfactory agreement between the DFT approach and GCMC simulation in estimation of the pore adsorption isotherm at 343 K. The former approach used the spherical carbon dioxide model, while the three-LJ-center model with partial charges placed on each site representing the carbon dioxide molecule was utilized in the GCMC simulation. Further, a carbon well depth of ϵ_c/k = 28 K was also employed in both the DFT-based calculations and the GCMC simulations. In this section, we compare predictions of carbon dioxide adsorption in Norit R1 extra carbon at 343 K using the FWT model with the corresponding experimental data (open circles) taken from Herbst et al.[58] As seen in Figure 12a and its inset, the FWT model significantly overpredicts the experimental data even in the low-pressure region (<10 MPa). This may be related to weaker fluid−wall interactions for polar compounds such as carbon dioxide due to crystalline defects and the presence of functional groups and/or a pore connectivity problem.[22,59] On the basis of the results in section 4.2.1, a pore connectivity problem is not expected for adsorption of carbon dioxide in Norit R1 extra carbon,

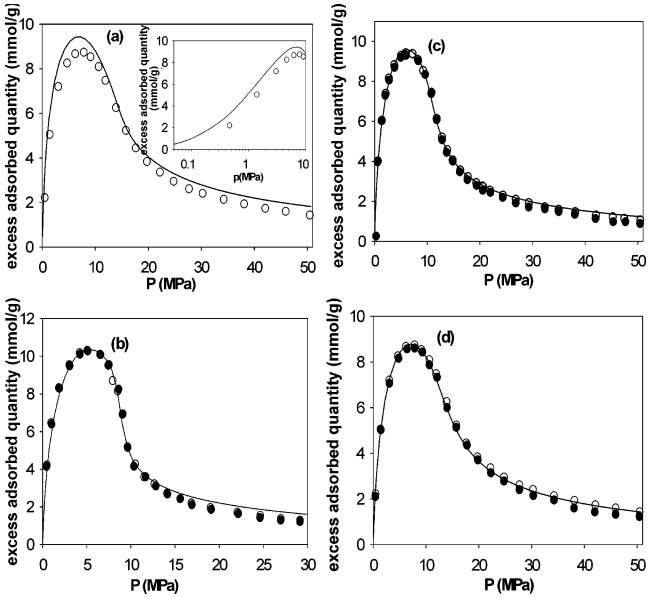

Figure 12. Predicted and experimental adsorption isotherms of supercritical carbon dioxide on Norit R1 extra carbon at various temperatures. The solid line depicts the predicted isotherm obtained from the FWT model using (a) the carbon well depth $\epsilon_c/k = 28$ and (b−d) the binary interaction parameter, k_{sf}, 0.093 67. The open circles depict experimental data taken from Herbst and Staudt,[58] and the filled circles are recalculated experimental data using the carbon volume, V_c, 0.465 cm^3/g: (a and d) 343 K; (b) 313 K; (c) 328 K.

as the FWT model predicts satisfactorily the adsorption of methane, whose effective molecular size is larger than that of carbon dioxide. Accordingly, the former reason related to crystalline defects and functional groups is anticipated for carbon dioxide. Further discussion on the pore network connectivity issue will be provided in a later section.

To verify the above arguments, we proceed to reduce the fluid−wall interaction parameter, ϵ_{cf}, to a value such that the predicted adsorption isotherm using the FWT model matches the corresponding experimental data at 343 K. This task is performed by utilizing the generalized Lorentz−Bertherlot mixing rule

$$\epsilon_{sf} = (1 - k_{sf})\sqrt{\epsilon_c \epsilon_f} \qquad (17)$$

where k_{sf} is the binary interaction parameter, considered as an adjustable parameter representing different wall−fluid interaction contributions from pure wall−fluid dispersion interaction.

It was found that a value of the binary interaction parameter, k_{sf} = 0.093 67, provided a good match between the predicted isotherm and the experimental data at 343 K, as seen in Figure 12d. Further, we employed this value of the binary interaction parameter (k_{sf} = 0.093 67) to predict the adsorption of carbon dioxide in the Norit R1 extra at 313 and 328 K. The results, depicted in parts b and c of Figure 12, respectively, show that the binary interaction parameter (k_{sf} = 0.093 67) consistently provides good agreement between the predictions using the FWT model and the corresponding experimental data up to 20 MPa, although the model slightly overpredicts the data at higher pressures. Such overprediction becomes more pronounced with decreasing temperature due to the fact that the density of the adsorbed phase exceeds the threshold of the bulk density region in which the DFT equation of state fits accurately experimental bulk data (Figure 5). Beyond this threshold density, the DFT

(58) Herbst, A.; Staudt, R.; Harting, P. *J. Therm. Anal. Calorim.* **2003**, *71*, 125.
(59) Lopez-Ramon, M. V.; Jagiello, J.; Bandosz, T. J.; Seaton, N. A. *Langmuir* **1997**, *13*, 4445.

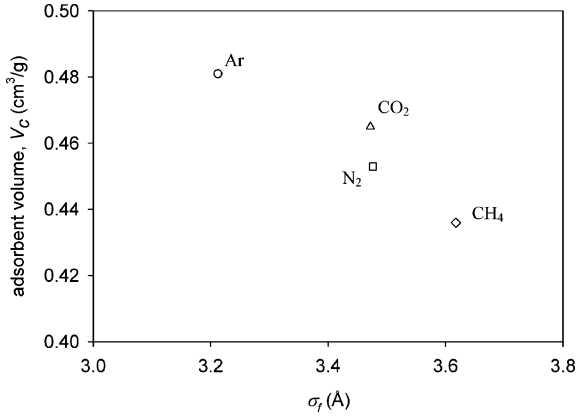

Figure 13. Variation in the value of adsorbent volume with molecular size, determined by different probing gases.

approach slightly overpredicts the GCMC simulated pore isotherms. Accordingly, the fitting to obtain adsorbent volume was based on agreement between the adsorption predictions and the experiments in the low-pressure range where adsorbed density does not exceed the threshold bulk density. The value of adsorbent volume ($V_c = 0.465$ cm^3/g) provides consistently good agreement between the FWT-based prediction and the experimental data at 343 K in the low-pressure range, where the DFT equation of state predicts accurately the bulk experimental density, and is also adequate at higher densities. The filled circles in Figure 12b and c represent recalculated experimental adsorption data using the new adsorbent volume ($V_c =$ 0.465 cm^3/g). Similar results to the adsorption prediction of carbon dioxide at 343 K are apparent.

Given the fluid interaction parameter, ϵ_f, that offers a good match between GCMC simulated or DFT equation of state calculated bulk isotherms and the corresponding experimental data for carbon dioxide, it appears that the binary interaction parameter, k_{sf}, varies quite significantly between different carbon types. In particular, Vishnyakov et al.[46] and Cracknell and Nicholson[42] showed that the use of the solid interaction parameter $\epsilon_s/k = 28$ K or the binary interaction parameter $k_{sf} = 0$ in GCMC simulation provides a proper prediction of experimental adsorption data on graphitized carbon blacks. In the current work, the binary interaction parameter for carbon dioxide, $k_{sf} = 0.093\,67$, accurately predicts the supercritical adsorption of carbon dioxide in Norit R1 extra carbon, as illustrated above. Accordingly, it is inferred that an increase in the binary interaction parameter from that of graphitic carbon for the case of carbon dioxide is due to the added contribution of electrostatic interaction arising from intermolecular interaction between multipoles of carbon dioxide and functional groups attached to the edge plane surface and/or basal plane. Such a contribution may be expected to influence the adsorption of carbon dioxide on the carbon surface. For instance, it may lead to a possible decrease in adsorbed quantity due to the preferential adsorption of carbon dioxide on the edge plane surface.[60] However, further systematic investigation on the adsorption of carbon dioxide on different carbon types from graphitic carbon to activated carbon must be conducted to confirm this finding. On the other hand, the value of the solid interaction parameter $\epsilon_s/k = 28$ K or the binary interaction parameter $k_{sf} = 0$ seems to predict satisfactorily the supercritical adsorption of nonpolar species such as argon and methane or very weakly polar species such as nitrogen, seen in the current work, as well as ethane[2], suggesting an advantage of utilizing such species as probe molecules for the characterization of porous carbons.

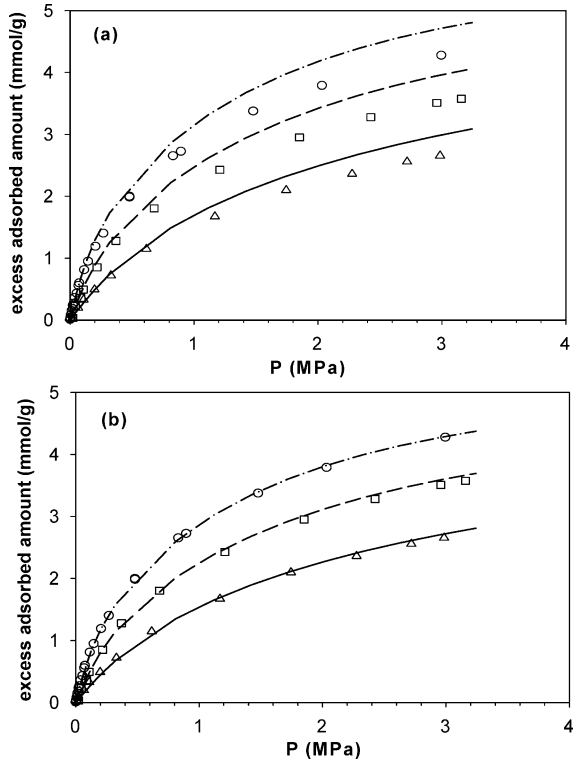

Figure 14. Predicted and experimental adsorption isotherms of supercritical methane on BPL carbon at various temperatures (308−373 K). The solid, dashed, and dashed−dotted lines depict the predicted isotherms at 373, 333, and 308 K, obtained using the FWT model. The symbols represent the experimental data taken from Gusev et al.,[62] (a) assuming complete accessibility of methane to the carbon pore space ($A_v = 1.00$) and (b) assuming partial accessibility of methane to the carbon pore space ($A_v =$ 0.91).

The slight increase in the value of the adsorbent volume with decreasing molecular size, found for the Norit R1 extra activated carbon in the above analysis using the different investigated gases, indicates different accessibilities of the investigated gases to the carbon surface. Such accessibility can be dependent in a complex way upon on fluid molecular size, fluid−wall and fluid−fluid interaction strengths, and solid surface roughness. In particular, it can be observed that the adsorbent volume of the Norit R1 extra carbon, V_c, determined from nonpolar or weakly polar compounds (Ar, N_2, and CH_4), indicates a good correlation with the molecular size of the gases, as seen in Figure 13, while carbon dioxide only slightly deviates from this correlation. Such observation is due to the different interaction nature of carbon dioxide to the carbon surface from that of the other investigated gases.

4.3. Connectivity Problem in Activated Carbon. The FWT model, as shown in the above sections, provides accurate predictions of high-pressure adsorption of argon, nitrogen, methane, and carbon dioxide on the BPL and Norit R1 extra carbons at various supercritical temperatures. However, it is interesting to find that the model overpredicts some other sets of adsorption measurements of methane in not only BPL carbon,[61,62] as seen in Figure

(60) Chen, S. G.; Yang, R. T. *Langmuir* **1993**, *9*, 3259.

(61) Reich, R.; Zeigler, W. T.; Rogers, K. A. *Ind. Eng. Chem. Process Des. Dev.* **1980**, *19*, 336.

(62) Gusev, V. Y.; O'Brien, B. J. A.; Jensen, C. R. C.; Seaton, N. A. *AIChE J.* **1996**, *42*, 2773.

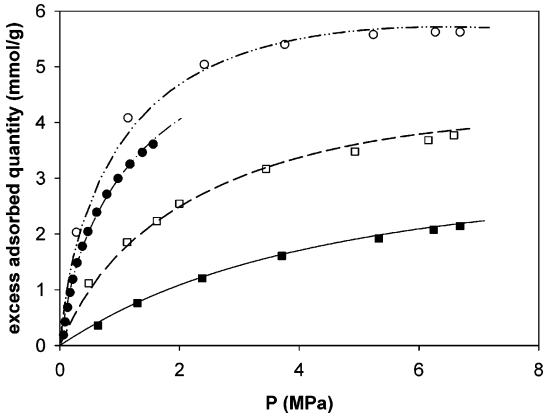

Figure 15. Predicted and experimental adsorption isotherms of supercritical methane on PCB carbon at various temperatures. The solid, dashed, dashed−dotted, and dashed−dotted−dotted lines depict the predicted isotherms at 480, 373, 313, and 296 K, obtained using the FWT model, assuming partial accessibility of methane to the carbon pore space ($A_v = 0.86$). The symbols represent the experimental data at 296 K (open circles), 373 K (open squares), and 480 K (filled squares) taken from Ritter and Yang et al.[63] and at 313 K (filled circles) taken from Choi et al.[64] The predicted isotherms are calculated using the FWT model.

14a, but also others such as PCB carbon.[63,64] This observation reveals the possible presence of inaccessible regions or a pore network connectivity problem in the examined carbons. There have been two possible interpretations of the network connectivity problem. The first interpretation is assigned to exclusion of large adsorbate molecules in the bulk phase from smaller pores of carbon internal structure. This interpretation has been investigated and refined by López-Ramón et al.[59] On the other hand, the exclusion of ethane molecules from the pore junction due to their incapability of turning sharply at a junction pore, as proposed earlier by Davies and Seaton,[22] provides a second interpretation. Further, the authors proposed modification of the existing GAI equation, eq 9, by introducing an additional term, A_v, representing the fraction of carbon volume accessible to the adsorbate. In particular, the modified equation is given as

$$\Gamma_{ex}(P) = A_v \int (\hat{\rho}(P, H_{in}) - \rho_b) f(H_{in})\, dH_{in} \qquad (18)$$

From the PSD results of the BPL and PCB carbons determined by the FWT model, as reported earlier,[1,2] it can be seen that the smallest pore size in the PSD results is larger than the molecular size of methane, suggesting inapplicability of the first interpretation of the pore network connectivity problem in the present case, while the second interpretation may apply. Accordingly, we fitted the theoretical adsorption isotherms of methane in the BPL and PCB carbons, calculated by the FWT model using eq 18, to the corresponding experimental adsorption data at various temperatures in the range 296−480 K on the same carbons. Here, the fraction of the accessible volume, A_v, arising from the assumption of same structural parameters (PSD and PWTD) in both accessible and inaccessible regions of carbon was taken as a constant fitting parameter. As seen in Figures 14b and 15, an excellent match between the theoretical adsorption isotherms and the corresponding experimental data is found. In particular, we find $A_v = 91\%$ for methane adsorption on BPL carbon and $A_v = 86\%$ for PCB carbon, regardless of temperature. Thus, the fraction of the accessible volume of methane, A_v, is temperature and pore size independent. The temperature independence of the parameter A_v can be expected for methane under supercritical conditions due to its quasi-symmetry and predominance of kinetic energy. Further, excellent prediction of methane adsorption with a constant fraction of accessible volume is consistent with the highly disordered nature of the examined carbons that yields structural uniformity in the carbons. Thus, it is clear that the significant variation of the internal structure of the BPL carbons between different batches, as mentioned earlier in the literature,[65] may be only due to their different pore junction structures, leading to added complexities in predicting gas adsorption equilibrium on the carbon, especially for linear molecules such as ethane due to the temperature dependence of their rotational motion.

5. Conclusions

In the current work, an extensive verification of the NLDFT approach against the GCMC simulation has been carried out for the pore adsorption equilibrium of simple gases (argon, nitrogen, and methane) as well as other gases such as carbon dioxide under supercritical conditions. For the simple gases, excellent agreement between the NLDFT approach and the GCMC simulation has been found for pore adsorption isotherms for pores whose size is >3.5 Å. However, a small deviation of adsorption isotherms, determined by the NLDFT approach, from the GCMC simulated results can be observed for small pores (<3.5 Å) due to the effect of the mean field approximation, utilized in the NLDFT calculations. For the more complex molecule carbon dioxide, satisfactory agreement between the NLDFT approach and GCMC simulations has been found for pore adsorption isotherms of most of the examined pore sizes at 343 K, although a discrepancy of at maximum 10% between the two approaches is observed for pore sizes ranging from 6.14 to 7.74 Å.

On the basis of good agreement between the NLDFT technique and the GCMC simulations for all the examined gases (Ar, N_2, CH_4, and CO_2) under supercritical conditions, successful predictions of the adsorption equilibrium of these supercritical gases on the various carbons (BPL, Norit R1 extra) over a wide range of temperatures by the FWT model using NLDFT calculated kernels have been achieved in the present work, proving reliable characterization of the porous carbons by the model. The success of the FWT model enables one to reliably ascertain the presence of pore network connectivity effects. This may not only help evaluate isotherms accurately but also improve the quality of activated carbons.

LA047545H

(63) Ritter, J. A.; Yang, R. T. *Ind. Eng. Chem. Res.* **1987**, *26*, 1679.
(64) Choi, B. U. *J. Chem. Eng. Data* **2003**, *48*, 603.
(65) Gusev, V. Y.; O'Brien, J. A. *Langmuir* **1997**, *13*, 2815.